Critical region of long-range depinning transitions

A. B. Kolton and E. A. Jagla

Comisión Nacional de Energía Atómica, Instituto Balseiro (UNCu), and CONICET Centro Atómico Bariloche, (8400) Bariloche, Argentina

The depinning transition of elastic interfaces with an elastic interaction kernel decaying as $1/r^{d+\sigma}$ is characterized by critical exponents which continuously vary with σ. These exponents are expected to be unique and universal, except in the fully coupled ($-d < \sigma \leqslant 0$) limit, where they depend on the "smooth" or "cuspy" nature of the microscopic pinning potential. By accurately comparing the depinning transition for cuspy and smooth potentials in a specially devised depinning model, we explain such peculiar limits in terms of the vanishing of the critical region for smooth potentials, as we decrease σ from the short-range ($\sigma \geqslant 2$) to the fully coupled case. Our results have practical implications for the determination of critical depinning exponents and identification of depinning universality classes in concrete experimental depinning systems with nonlocal elasticity, such as contact lines of liquids and fractures.

I. INTRODUCTION

Many dissipative disordered systems display a collective depinning transition, from an almost static (or inactive) to a sliding (or active) regime at a threshold value of a driving force. Examples range from field-driven domain walls in ferromagnetic [1–3] or ferroelectric materials [4,5], crack propagation under stress in heterogeneous materials [6,7], contact lines of liquids on a rough substrate [8–10], imbibition of fluids in porous and fractured media [11], reaction fronts in porous media [12], solid-solid friction [13], sheared amorphous solids or yield stress fluids [14], dislocation arrays in sheared crystals [15], current-driven vortex lattices in superconductors [16–18], skyrmion lattices in ferromagnets [19], to even collective cell migration during wound healing or cancer invasion [20]. The collective nature of the depinning transition is often spectacularly manifested at low temperatures through some kind of "crackling noise" which, well beyond the laboratory scale, much resembles earthquakes, motivating also their study within the very same framework [21,22].

A very fruitful analogy of this problem with equilibrium phase transitions emerges when considering the driving force as the control parameter and the mean sliding velocity as the order parameter. This analogy has been useful in pointing out directions for seeking universal behavior and inspiring new methodologies [23,24]. The analogy has also been useful to point out the relevance of genuine nonequilibrium effects [25], and to detect nonstandard features of the transition [26–28]. Among the very different models that can be proposed, the depinning transition of elastic manifolds in random media has become a paradigmatic basic problem, as it presents the essential ingredients for a nontrivial universal behavior, together with an advantageous combination of analytical [29–32] and numerical [33,34] tractability. Moreover, it is directly relevant for predicting universality classes of various concrete systems where the elastic approximation can be justified, notably magnetic domain walls and contact lines of liquids menisci.

The depinning transition at zero temperature of an overdamped elastic interface in a random potential is continuous, nonhysteretic, and occurs at a characteristic threshold force f_c. Close enough and above the threshold, the mean velocity v of the interface in the direction of the force is well described by the putative depinning law $v \sim (f - f_c)^\beta$, with β a nontrivial critical exponent. A divergent correlation length $l \sim (f - f_c)^{-\nu}$ and a divergent correlation time $\tau \sim l^z$ characterize the jerky motion as we approach f_c from above. Concomitantly, the rough geometry of the interface becomes self-affine, with the displacement field growing as $u \sim x^\zeta$ for length scales x below l. Hence $v \sim l^{\zeta - z}$ and $\beta = \nu(z - \zeta)$. In this regime, the spatiotemporal fluctuations also display universal behavior and are controlled by avalanches with a broad distribution of sizes S (and durations $T \sim S^{z/(1+\zeta)}$), such that $P(S) \sim S^{-\tau}$, with $\tau = 2 - (\zeta + 1/\nu)/(d + \zeta)$ in the quasistatic limit. The critical exponents can be calculated in an ϵ expansion [29–31,35,36] and also found numerically [33,37–41] to determine the different universality classes. These are determined by d, the range [42–46] or nature [47] of the elastic interactions, the anisotropic [48] or isotropic correlations of the pinning force [49,50], and by the presence of additional (i.e., apart from the pinning force) nonlinear terms [25,48,51–54]. Boundary- [55] or ac-driven [56] depinning of elastic interfaces has been also studied. If the so-called statistical tilt symmetry holds, only two exponents are needed to fully characterize the depinning universality class. In any case, it is very convenient to consider separately the purely geometric ζ or ν, which do not involve time scaling, from z or β which do.

In order to quantify the universal properties of the depinning transition for a concrete experimental system (or microscopic model with a yet unknown coarse-grained dynamics) it is important to determine the critical exponents accurately enough so as to be able, at least, to differentiate between different candidate universality classes. Unfortunately, testing the depinning law is in general a rather difficult task experimentally, and in many cases also numerically. On one hand

[57], fitting accurately β certainly requires an accurate estimation of the nonuniversal threshold force f_c. In that respect it is important to note that the depinning force f_c displays important sample-to-sample fluctuations in finite systems [58], with $\overline{[f_c - \overline{f_c}]^2} \sim L_0^{-2/\nu_{FS}}$, where L_0 is the linear size of the system and $\nu_{FS} \geqslant 2/(d + \zeta)$ [35]. The thermodynamic limit $L_0 \to \infty$ is also delicate, as the value of f_c can be strongly affected by the anisotropic sample aspect-ratio scaling we keep in such limits [58,59]. On the other hand, even if we are able to get a sharply defined f_c, we are faced with the fact that the depinning law is expected to hold only in an unknown critical region of size $\sim \Delta f^{\mathrm{crit}}$, such that the asymptotic power-law scaling for v fully develops only for $(f - f_c) \lesssim \Delta f^{\mathrm{crit}}$. Knowing roughly Δf^{crit} is thus fundamental for practical applications of the theory. Little is known, however, about Δf^{crit} for the depinning transition, except that it is nonuniversal and may be small in practice, as noted already in pioneer works [31,33]. How does the critical region depend on the microscopic shape of the disorder, the range of the elastic interactions, or the dimensionality d? Do scaling corrections produce intermediate power laws with effective exponents? If so, are the effective exponents expected to be larger or smaller than the true ones? Do they violate the expected asymptotic scaling relations among exponents?

In this paper we try to answer some of the above-mentioned practical questions by performing numerical simulations on different microscopic models. We study depinning models with isotropic uncorrelated disorder and harmonic long-range elasticity, with the elasticity kernel decaying with distance as $1/r^{d+\sigma}$. We vary the range of the elastic interactions from the ($\sigma \leqslant 0$) fully coupled case to the ($\sigma \geqslant 2$) short-range cases and compare the critical behavior of the velocity-force characteristics for two different forms of the microscopic disorder. They are termed the "smooth" case (in which the force originating in the disorder does not have any discontinuities) and the "cuspy" case (in which the force has an abrupt jump at the transition point between different potential basins). For the cuspy potential the extent of the critical region tends to be large and rather independent of the value of σ. For the smooth potential the critical region where universality holds (i.e., where we get the same exponents as in the cuspy case) decreases by increasing the range of elastic interactions and strictly vanishes, $\Delta f^{\mathrm{crit}} \to 0$, in the fully coupled limit. In such limit scaling corrections are no longer "corrections" but control the ultimate asymptotic scaling. This explains the peculiar nonuniversality of the fully coupled model in the strong pinning phase (i.e., with $f_c > 0$), which displays two different exponents, $\beta = 3/2$ and $\beta = 1$, for the smooth and cuspy cases, respectively. For $\sigma > 0$, where a unique value of β is the "right" one [60], our results show nevertheless the great importance of scaling corrections and the emergence of dangerous effective power laws, which particularly affect the obtention of the asymptotic dynamical exponents β or z as compared with the roughness exponent ζ, which is found to be more robust. These corrections are particularly relevant for a successful experimental (and also numerical) identification of depinning universality classes in elastic systems with long-range interactions ($0 < \sigma < 2$) and to explain quantitative discrepancies with theory.

To arrive at these results and emphasize their practical consequences, we devise a convenient model for comparing the critical behavior of cuspy and smooth microscopic disorders accurately. We focus on the $d = 1$ model with long-range interactions (the $d > 1$ short-range case will be discussed in the Appendix). First, in Sec. II the numerical model is presented. Then in Sec. III A results are presented for both smooth and cuspy microscopic pinning potentials. These results allow us to illustrate the kind of effects that can be expected in the critical region for $\sigma > 0$ in both cases. In Sec. III B we look in detail into the critical region by proposing an alternative model to compare the two different forms of pinning potential using discrete displacements and an effective microscopic potential described by traps and suitable transition rates. In Sec. V we summarize our results and discuss their practical implications for the study of the depinning transition.

II. GENERALITIES OF THE BASIC MODEL

We model a d-dimensional interface embedded on a $d + 1$ disordered material as a collection of blocks $i = 1, \ldots, N$, located at sites of a d-dimensional regular lattice and characterized by a continuous displacement $u_1, \ldots, u_N$ in the $d + 1$ transverse direction. We will assume an overdamped equation of motion,

$$\dot{u}_i(t) = \sum_{j=1}^{N} G_{ij}(u_j - u_i) + F_i(u_i) + f, \qquad (1)$$

where the terms on the right-hand side represent the sum of the elastic couplings, the disorder, and the uniform and constant pulling force, respectively.

The G term in Eq. (1) accounts for the harmonic elastic interactions, with G_{ij} being the spring constant associated with the blocks i and j. In order to model long-range elastic interactions we use $G_{ij} = \kappa/|i - j|^{d+\sigma}$, with the normalizing constant κ used to obtain $\sum_j G_{ij} = 1$. [Note that the value of G_{ii} does not influence Eq. (1) and is taken as zero.] The G term just described implies the convex elastic energy $\sum_{ij} G_{ij}(u_i - u_j)^2/2$.

When $\sigma \geqslant 2$ the elastic kernel represents a short-range elastic interaction, while for $-d < \sigma \leqslant 0$, it represents the fully coupled case that can be exactly solved using mean field techniques. Periodic boundary conditions can be taken into account by summing the elementary kernel over periodic images of the finite system and by using its Fourier representation to obtain the elastic forces at each step of time integration through a numerically efficient convolution.

The second term in Eq. (1) (the only nonlinear term of the equation of motion) accounts for the pinning forces. For the moment we will just assume it is statistically characterized by $\overline{F_i(u)} = 0$, $\overline{F_i(u)F_j(u')} = \Delta(u - u')\delta_{ij}$, where $\overline{\cdots}$ stands for the average over disorder realizations and $\Delta(u)$ is a short-ranged function with $\Delta(0)$ measuring the strength of the disorder.

The motion described by Eq. (1), with its convex elastic energy, is characterized by a unique critical force f_c in the large-size limit [61]. This critical force is important in determining the fate of the system at very long times.

If $f < f_c$ the system reaches a static solution such that $\dot{u}_i(t) = 0 \; \forall i$. For $f > f_c$ it reaches a unique steady state with $\dot{u}_i(t) \geqslant 0$ univocally defined up to a global time shift, with the mean velocity defined as $v \equiv N^{-1} \sum_{j=1}^{N} \dot{u}_i(t)$ or by $v \equiv \lim_{t \to \infty} (Nt)^{-1} \sum_{j=1}^{N} [u_i(t) - u_i(0)]$, thanks to self-averaging. The properties just described are consequences of the Middleton theorems [62] which assure that the dynamics described by Eq. (1) with its convex elastic energy converges for $f \geqslant f_c$ to a unique "Middleton attractor." The properties of this attractor can be exploited to devise smart algorithms to target the critical force and critical configuration in finite samples without solving the true dynamics [63,64]. It also allows one to cleanly visualize the convergence towards the steady state by reparametrizing the time with the system center of mass $u(t) \equiv N^{-1} \sum_{j=1}^{L^d} u_i(t)$ [65]. In this paper we will rely (apart from the unicity of the dynamical attractor) on the general property $\dot{u}_i(t) \geqslant 0$, valid in the $f \geqslant f_c$ steady state. This will be particularly important in relation to the model discussed in Sec. III B.

It is also worth remarking here that the so-called statistical tilt symmetry (STS) holds for Eq. (1), so $\nu = 1/(\sigma - \zeta)$ for $d/2 \leqslant \sigma \leqslant 2$, $\nu = 1/(2 - \zeta)$ for $\sigma \geqslant 2$, and $\nu = 1/2$ for $\sigma < d/2$ [24]. Therefore only two exponents are needed to fully characterize the depinning universality class [66] The discussion of anisotropic depinning universality classes, where STS is broken will be published elsewhere. Nevertheless, we believe that our general conclusions hold also for this case. Using the STS, in this work we will consider separately ζ and β to characterize the universality classes. As we will discuss later, this arbitrary separation is nevertheless quite convenient, as ζ (and ν) has a purely geometric origin unlike β (and z), which are related with time scaling and thus affected by local nonuniversal bottlenecks. This has important consequences from a practical point of view. For instance, it is easier to get much more accurate values for ζ (or ν) by exploiting different methods which do not involve a true temporal evolution, such as the variant Monte Carlo algorithm [63,64] or the metastable configurations obtained by relaxing a flat configuration below the depinning threshold [67].

For $f \gg f_c$ the effect of the disorder can be treated as a perturbation. At first order disorder mimics an effective temperature proportional to v^{-1}. In this so-called "fast flow" regime the interface can be fairly described by the forced Edwards-Wilkinson equation [68] and $v \approx f$ [69]. For the low velocity critical regime $f \gtrsim f_c$ we are interested in, perturbation theory fails. Numerical simulations and the functional renormalization group (FRG) approach applied to Eq. (1) teach us that, for $\sigma > 0$, the above description uniquely determines the critical depinning exponents of the model. Their values depend on d, and smoothly evolve with decreasing σ, from their short-range values for $\sigma \geqslant 2$ to the mean field value for $\sigma \leqslant d/2$ or equivalently, $d \geqslant d_c(\sigma)$, with $d_c = 2\sigma$ the upper critical dimension [70]. The exact "shape" of the microscopic pinning force F_i is believed to be unimportant in many respects. Indeed, FRG tells us that for the model of Eq. (1), the bare correlator of the pinning force $\Delta(u)$ flows under coarse graining above the fundamental Larkin scale L_c towards a correlator with a "cuspy" singularity. The existence of such a cusp nicely accounts for the existence

of a critical force and also for the existence of avalanches. The fixed point of the renormalization flow equations for the pinning correlator function gives us access to unique values of $\beta \equiv \beta(d, \sigma)$ and $\zeta \equiv \zeta(d, \sigma)$, which completely characterize the depinning universality class of our model. These FRG calculations are performed assuming in principle a small separation $\epsilon \ll 1$ from the upper critical dimension, $\epsilon = d_c(\sigma) - d$, with $d_c = 2\sigma$. One may thus question their validity for the experimentally relevant case $d = 1$, for instance. Numerical simulations by Rosso *et al.* [40] fairly confirm, however, the FRG picture for one-dimensional interfaces with short-range elastic interactions ($\sigma \geqslant 2$), showing its validity for the extreme $\epsilon = 3$ case.

The above picture, valid for $\sigma > 0$ and in principle any dimension $d \geqslant 1$, sharply contrasts with the $\sigma \leqslant 0$ fully coupled limit, where the depinning model becomes equivalent to the exactly solvable one-particle Prandtl-Tomlinson model, one of the most popular models in nanotribology [71]. For the strong pinning phase of this model, which has $f_c > 0$ (see, e.g., Ref. [72]), the critical behavior of the velocity $v \sim (f - f_c)^\beta$ becomes nonuniversal for different microscopic potentials. On one hand, for a smooth random potential V_i such that $F_i(u) = -(d/du)V_i(u)$ does not have jumps, one has $\beta = 3/2$. On the other hand, for a cuspy random potential with force discontinuities $\beta = 1$ is obtained, a value that coincides with the mean field value expected from FRG for $d \leqslant d_c(\sigma)$. We will concentrate in explaining this unusual behavior. As we will see, the explanation implies for smooth potentials the progressive reduction of the extent of the critical region as $\sigma \to 0$. In turn, this will prove to have practical consequences when addressing the experimental determination of critical exponents in systems evolving on smooth pinning potentials.

III. RESULTS

A. Numerical results: Continuous potentials

We will present results of direct numerical simulations of Eq. (1) to have a first clear picture of the differences that appear between smooth and cuspy pinning potentials. In concrete, the numerical potentials we used are defined as follows (see Fig. 1). For each site i a potential $V_i(u_i)$ is constructed. The generic potential $V(u)$ is constructed piecewise by dividing the u axis in segments through a set of values a_n. In each interval a_n-a_{n+1} (defining $\overline{a} \equiv (a_{n+1} + a_n)/2$ and $\Delta \equiv a_{n+1} - a_n$) the potential is defined as

$$V(u) = [(u - \overline{a})^2 - (\Delta/2)^2] \qquad (2)$$

for the cuspy case and

$$V(u) = -\frac{3\Delta^2}{2\pi^2}\left[1 + \cos\left(\frac{2\pi(u - \overline{a})}{\Delta}\right)\right] \qquad (3)$$

for the smooth case. Note that even in the smooth case the potential is not analytic, but it has a continuous second derivative, which is enough for our purposes. The separation Δ between a_n and a_{n+1} is stochastically chosen from a flat distribution between $\Delta_{\min} = 1$ and $\Delta_{\max} = 2$.

Equation (1) is integrated using a first-order Euler method with a time step of 0.1. The results are obtained starting at large values of applied f and progressively reducing it until the critical force f_c is reached when the velocity drops to
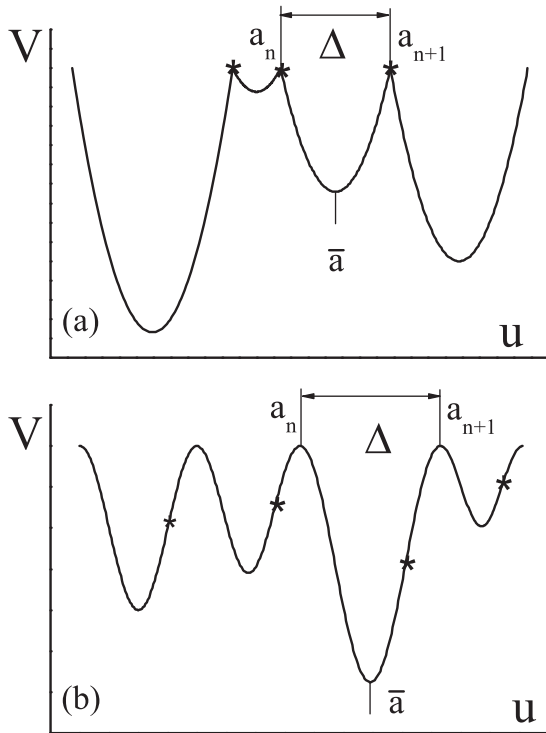
FIG. 1. Typical forms of the pinning potentials we analyze. Transition points for a particle moving to the right are indicated by stars. (a) A cuspy potential, in which there is a jump of the force at the transition point. (b) A smooth potential, in which the potential itself and its derivatives (up to second order at least) are continuous.
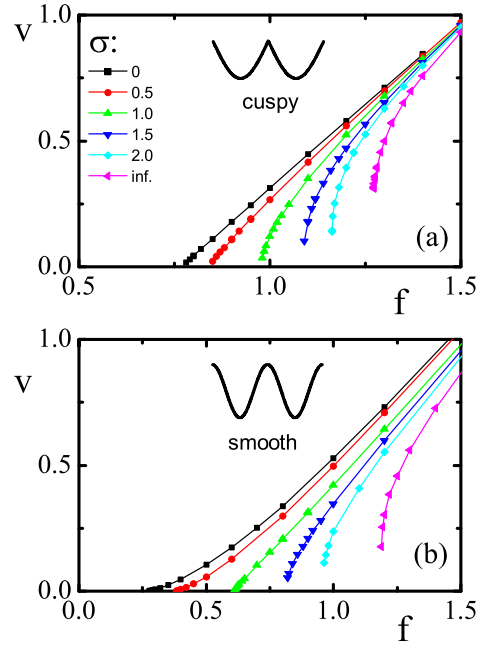

FIG. 2. Velocity as a function of force for a system of $N = 2^{16}$ sites, for different values of σ, using cuspy (a) and smooth (b) pinning potentials. Curves with the same value of σ display apparently larger values of β in (b) than in (a).

To overcome this difficulty and try to set this point, we have done simulations in a modified model that is described in the next section.

B. Numerical results: Discrete pinning potential

The results for the flow curves contained in the previous section (Figs. 2 and 3) suggest that there are strong nonuniversal effects associated to the form of the pinning potential that is used. These nonuniversal effects can mask the true critical behavior (that must be independent of the form of the potential for $\sigma > 0$), and so they have a great practical importance. Yet to determine accurately the behavior close to the critical force f_c we face the problem mentioned at the end of the previous section: The value of the critical force is not known in advance, and it has to be determined during the fitting
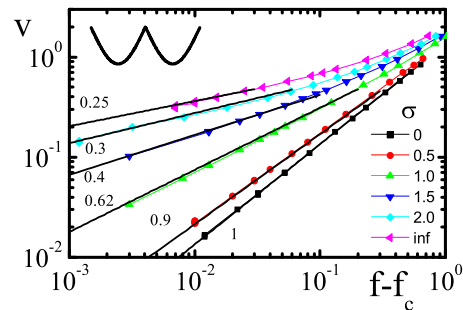
zero. In Fig. 2(a) we see the value of v as a function of f for the case of cuspy potentials for a few values of σ going from nearest neighbor interaction ($\sigma \to \infty$) to mean field interaction ($\sigma \to 0$). The plot in logarithmic scale with respect to the critical force f_c (Fig. 3) (fitting in each case the value of f_c) displays a robust critical region in which the β exponent can be defined. The value of β as a function of σ (reported also in Fig. 3) increases when σ moves from large values to $\sigma = 0$. Moreover, the actual values of β obtained for different σ accurately fit those known from the literature [73]. This represents the "standard" behavior that is compatible with the analysis using renormalization group techniques.

The results of simulations using smooth potentials are shown in Fig. 2(b). They show apparently larger values of β than the values for cuspy potentials at the same σ [Fig. 2(a)]. For instance, the curve for $\sigma = 1$ seems to have a slope close to 1, instead of displaying $\beta \simeq 0.62$ as in the cuspy case.

As we have anticipated, the way out of this conundrum is to realize that the critical region at which the results for smooth potentials should coincide with those of cuspy potentials may be small and we might not be observing it in Fig. 2(b). The critical region should become observable when plotting the results of Fig. 2(b) in logarithmic scale with respect to the critical force f_c. However, the identification of the critical region and the true value of β relies on the accurate determination of the value of f_c, and this has to be done at the same time as fitting the value of β, so it is very difficult to get reliable values of β if the critical region is expected to be very small.

FIG. 3. The data in Fig. 2(a) plotted in logarithmic scale, fitting the critical force for each value of σ. The value of the β exponent is obtained as the slope of the asymptotic straight behavior, as indicated.

process itself. This may be quite inconvenient when the extent of the critical region is very small, as a slight uncertainty in the critical force can completely alter the results in this critical region.

In this section we present a modification of the model used previously Sec. III A that does not have this drawback and allows a more precise characterization of the effects we are studying. In addition, it also allows a very precise determination of other exponents of the transition, in particular, the dynamical exponent z, something that we are also interested in.

The modified model has been used to study thermal creep in Ref. [28] and also in the context of earthquake dynamics [22], where it was termed the *narrow wells approximation*. It is obtained in the following way. Referring to Fig. 1, imagine that instead of an immediate concatenation of parabolic or cosinusoidal pieces we introduce flat portions of potential between consecutive wells. In the limit in which the wells are narrow compared to the intervening flat regions and very deep, the interface can only be pinned at the (now discrete) positions of the wells. Each well is characterized by a threshold force f_i^{th} for the interface to escape from it. (For simplicity in the simulations we take the values of f_i^{th} as constant: $f^{\mathrm{th}} = 2.5$.) The next step is to avoid the full simulation of the transition when the interface is jumping from one well to the next. The transition is supposed to occur in a single time step, but taking into account the time the transition takes in the original model. To introduce the transition rates we use, we first define the applied force f^{app} at site i as

$$ f_i^{\mathrm{app}} = \sum_{j=1}^{N} G_{ij} (u_j - u_i) + f. \tag{4} $$

The interface jumps between successive discrete positions (that are taken completely random, with an average separation of 0.1) when f_i^{app} exceeds the local critical force f_i^{th}. The jump itself is considered to be instantaneous (it takes a single time step), but the transition between consecutive positions does not occur immediately after the critical force is exceeded. Instead, a transition rate is considered. Cuspy and smooth cases of the model in the previous section differ qualitatively in the time it takes for a particle that has exceeded the stability limit of one potential well to reach the next equilibrium point at the next well. In the case of cuspy potentials this time is roughly constant, independent of the extent by which the threshold force has been exceeded. In the case of smooth potentials this time goes as $\sim (f^{\mathrm{app}} - f^{\mathrm{th}})^{-1/2}$, typical of saddle-node bifurcations. We can model this behavior by assigning a constant transition rate $\lambda \sim \mathrm{cte}$ to mimic the effect of cuspy potentials (this will be referred to as the "constant rate" case) and a rate that depends on applied force as $\lambda \sim (f^{\mathrm{app}} - f^{\mathrm{th}})^{1/2}$ to simulate the case of smooth potentials (referred to as the "variable rate" case) [74]. In the concrete implementation, we consider all unstable sites for which $f_i^{\mathrm{app}} > f_{\mathrm{th}}$ and calculate an expected time τ_i for each site to jump, taken from a Poisson distribution with the corresponding rate λ_i. The lowest of all τ_i is chosen and this is the site that is actually moved. Time is advanced by this minimum τ_i, elastic forces are recalculated, and the process is continued. Average velocity is simply calculated
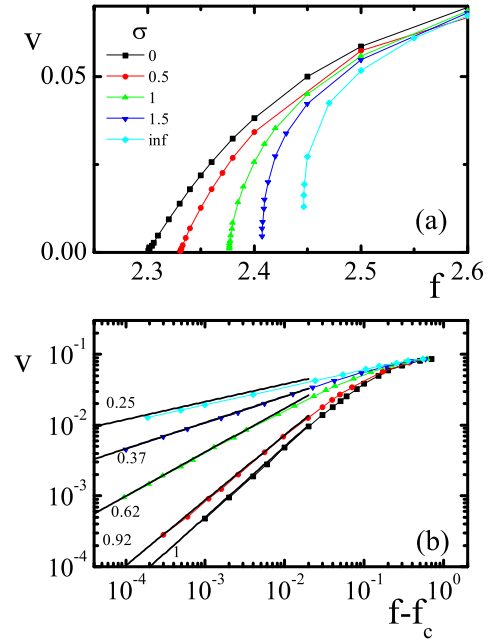

FIG. 4. (a) Flow curves of the discrete pinning potential model with constant transition rate for different values of σ. (b) Same data in logarithmic scale, fitting the value of f_c in each case. From these curves the value of the β exponent can be determined.

as $[u(t) - u(0)]/t$ in a run over a long time interval t. Note that although the positions of the interface are discrete, the dynamics is still continuous time, and no more that a single site is assumed to jump at each time step.

The advantage of the discrete potential model is that its quasistatic properties are completely independent of the rate law that is used. In fact, let us consider, for instance, two avalanches in the system that start from the same configuration but that evolve according to two different rate laws. Since the effect of any forward jump of any portion of the interface is to increase the force over any other site in the system, the avalanches will be exactly the same whatever the rate law is; the only possible difference is in the order and time of activation of different sites, by virtue of the Middleton theorems. This means at once that all static critical exponents such as τ, ζ, ν... must be independent of the rate law. In addition, the critical force will also be independent of the rate law, which is very convenient from the point of view of accuracy of the simulations, as explained previously. The only exponents that can depend on the rate law are those that sense temporal properties of the dynamics. They are the flow exponent β and the dynamical exponent z.

The flow curves obtained at constant rate for different values of σ are shown in Fig. 4. There is a clear difference in the flow curves between Figs. 4 and 2 for large values of f, which is a consequence of the details of the models. (The discrete pinning model does not have a "fast flow" regime, but a velocity saturation at large forces.) However, the values of the β exponent determined from the logarithmic plots [panel (b)] are in excellent agreement with those in Fig. 3, showing that the discrete model with constant rate in fact reproduces the behavior of the continuous cuspy pinning potential.
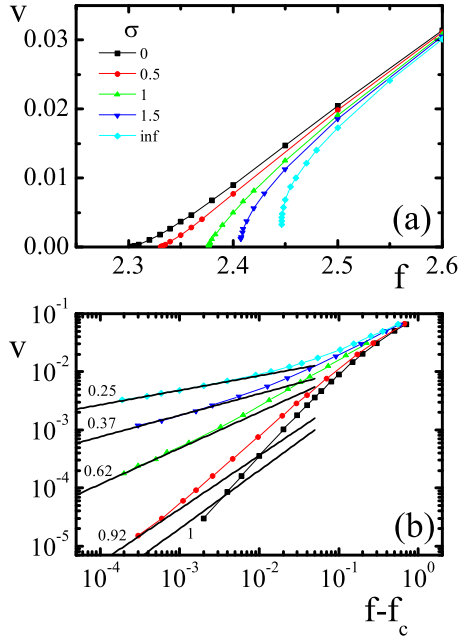
FIG. 5. (a) Flow curves of the discrete pinning potential model with rate transition λ that depend on stress as $\lambda \sim (f^{\mathrm{app}} - f^{\mathrm{th}})^{1/2}$, for different values of the long-range interaction exponent σ. (b) Same data in logarithmic scale, using the value of f_c previously used in Fig. 4(b). The continuous straight lines have the same slope than in the previous figure.

Figure 5(a) displays the flow curves in the variable rate case, namely, $\lambda \sim (f^{\mathrm{app}} - f^{\mathrm{th}})^{1/2}$, mimicking the smooth continuous potential case. Comparing Figs. 5(a) and 4(a) we observe again [as between Figs. 2(a) and 2(b)] a clear difference in the overall form of the curves with values of β that look larger in Fig. 5(a) than in Fig. 4(a). In order to quantify this difference in more detail it is necessary to look close to the critical force. It was already mentioned that the great advantage of the discrete pinning model is that the values of critical force for the curves in Fig. 5(a) are the same values as for the curves in Fig. 4(a), which were already fitted to construct Fig. 4(b). Using those values we construct the plot in Fig. 5(b). We note that as far as $\sigma > 0$ the curves eventually reach the same exponent than in Fig. 4 when approaching the critical force. However, the force range in which this limiting behavior is obtained shrinks as σ is reduced, and we are actually unable to observe it clearly once $\sigma \lesssim 0.5$. Our conclusion is that the critical region with the same β as in the constant rate case remains finite for all $\sigma > 0$ but shrinks as σ is reduced, vanishing for $\sigma \leqslant 0$, where the mean field value $\beta = 3/2$ is reobtained.

An alternative way to look at the effect just described is to plot the ratio R between the velocities for variable and constant rates. (Note that this makes sense only in the present case in which the critical force is the same for the two different rates.) The results contained in Fig. 6 show a remarkable systematic trend. As a function of $\Delta f \equiv f - f_c$, the velocity ratio R behaves as $R \sim C + A\Delta f^{1/2}$. The value of A is almost independent of the long-range interaction exponent σ, but C has a systematic dependence, reducing as σ decreases, and vanishing at $\sigma = 0$. For any $\sigma > 0$ the finite value of
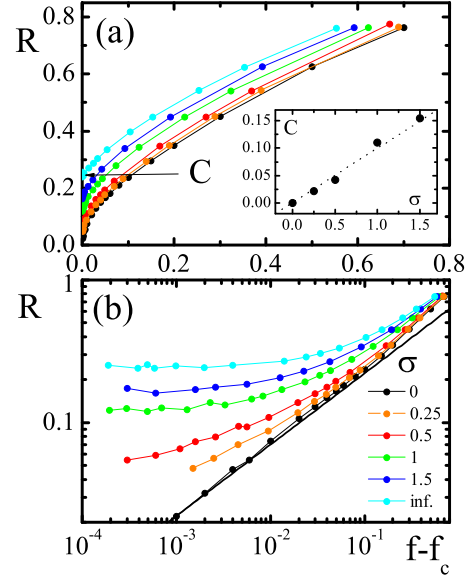

FIG. 6. Ratio R between the velocities for variable and constant rate as a function of the separation from the critical force. Linear (a) and logarithmic (b) scales. The limiting value C for $f - f_c \to 0$ is plotted in the inset.

C implies the coincidence of the β values for constant and variable rate. However, as C decreases, the range to observe this coincidence decreases also, and for $\sigma = 0$ (i.e., $C = 0$) the value $\beta = 3/2$ is obtained for variable rate, instead of the $\beta = 1$ that is obtained for the constant rate.

The estimation we have for R allows us to quantify the extent of the critical region. We can say that the critical region extends roughly up to the point where $C(\sigma) \sim A\Delta f^{1/2}$. This provides $\Delta f^{\mathrm{crit}} \sim C(\sigma)^2$. As C is observed to be roughly linear with σ, we finally obtain $\Delta f^{\mathrm{crit}} \sim \sigma^2$.

IV. IMPLICATIONS ON THE AVALANCHE DYNAMICS

The discrete pinning potential model is also useful to make an accurate determination of avalanche statistics. In order to analyze it, we did simulations using a quasistatic algorithm that keeps the system at the critical force at the same time that a collection of independent avalanches is generated. The algorithm consists in adjusting dynamically the value of the applied force in the following way. Suppose we start with a stable configuration ($f_i^{\mathrm{app}} < f_i^{\mathrm{th}}$ for all i). At this point, f is increased to the point where for some j we get $f_j^{\mathrm{app}} = f_j^{\mathrm{th}}$, and therefore an avalanche starts at site j. For every jump from u_i to $u_i + \delta$ within the avalanche, external force f is reduced to $f - \delta/N$. In this way, f eventually becomes lower than f_c and the dynamic stops. This is the end of the avalanche. Avalanche size S (calculated as the difference between $\sum_i u_i$ after and before the avalanche), avalanche duration T (defined as the sum of all activation times within the avalanche [75]), and spatial extent L (which is the number of sites that jumped at least once during the avalanche) are recorded. Then applied force f is increased again and the process is repeated. The statistical behavior of these three quantities allows us to determine some important critical exponents of the transition. For instance, the (average)
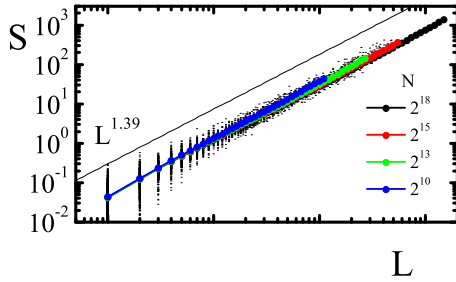
FIG. 7. Size S vs spatial extent L of individual avalanches (small dots) obtained in quasistatic simulations of the discrete pinning potential model, at $\sigma = 1$. Averaging over small L intervals the continuous lines are obtained for different system sizes, which allows one to determine the value of the critical exponents ζ. The value obtained $\zeta \simeq 0.39$ coincides with the one reported in the literature.

relation between S and L allows us to determine the roughness exponent ζ through $S \sim L^{d+\zeta}$. In addition the relation between T and L determines the dynamical exponent z: $T \sim L^z$.

In Fig. 7, S vs L is plotted for the "standard" long-range case $\sigma = 1$, which is particularly relevant for propagating fractures, contact lines of liquids or "magnetically charged" domain walls [43]. By construction of the model, this plot is valid both for constant and also for variable rates. Although the individual data points are quite scattered, averaging over small intervals of L allows us to obtain a good estimation of ζ. The value obtained ($\zeta \simeq 0.39$) perfectly coincides within the error bar with the value reported in the literature (see, e.g., Ref. [44]).

We now focus on the duration T vs spatial extent L relation, determining the dynamical exponent z as $T \sim L^z$. This result depends on the form of the rates. For constant rate the result is shown in Fig. 8(a) and is consistent with the expected value of z, namely, $z \simeq 0.77$ [42,45]. The results in Figs. 7 and 8(a) further support the claim that the constant rate discrete pinning potential is a realization of the cuspy continuous potential case.
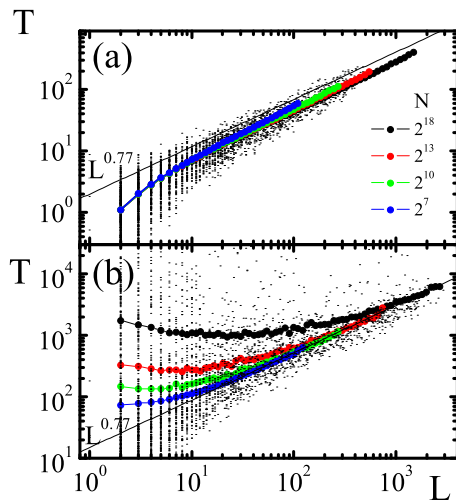

FIG. 8. Duration vs spatial extent of avalanches obtained in quasistatic simulations of the discrete pinning potential model with constant (a) and variable (b) transition rate, at $\sigma = 1$.
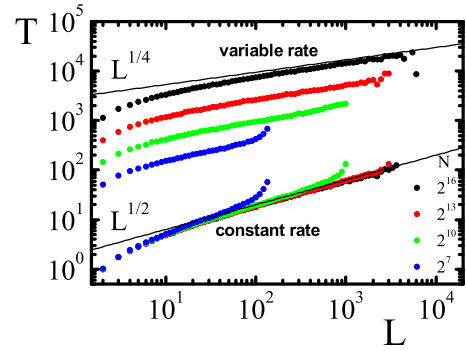

FIG. 9. Duration vs spatial extent of avalanches obtained in quasistatic simulations of the discrete pinning potential model, in a mean field situation ($\sigma = 0$). For constant transition rate the expected result $z = 1/2$ is obtained, and there are no dependences on system size besides the appearance of progressively larger avalanches as system size increases. For a variable transition rate the value $z = 1/4$ is obtained and in addition, a global dependence on system size of the form $N^{1/2}$ is observed.

The results for T vs L for the variable-rate case are presented in Fig. 8(b). The first thing that is observed is that data for individual avalanches (small dots) are much more scattered compared to Fig. 8(a). This behavior is clearly related to the variable rate: whereas for constant rate the avalanche duration is at most of the order of avalanche size, for variable rate even small avalanches can last for quite long, as a single site may take a very long time to be activated if it is only slightly above the local critical force. The next observation in Fig. 8(b) is that a relation $T \sim L^z$ with z being the same exponent as in Fig. 8(a) is obtained, but only for sufficiently large avalanches. This is in fact consistent with our view that the critical region for the variable rate case is much smaller than for the constant rate case, and only large avalanches display the correct critical T vs L dependence. For small avalanches this dependence deviates towards larger values of T. Interestingly, cracks experiments [6] also show an "excess duration" for small avalanches, suggesting the nonuniversal effect of smooth microscopic disorder or "variable rate" local instabilities. Note also that for these small avalanches the typical duration depends also on the system size N, an effect that was already discussed in Ref. [76] in the context of the yielding transition.

Since the results for the flow curve support the idea that the size of the critical region shrinks to zero as $\sigma \to 0$, the question naturally arises as to what is the nature of the T vs L dependence and the value of z in this limit, for constant and variable rates. To address this point we generated avalanches in a mean field case ($\sigma = 0$) and plot the results in Fig. 9, both for constant and variable rate, for a system of different sizes. The results for constant rate are consistent with the standard value of z in mean field, namely, $z = 1/2$. However, results for variable rate sharply deviate from this behavior. We obtain a value of $z = 1/4$ instead, and also an overall dependence on the system size, in such a way that we can write $T \sim L^{1/4}N^{1/2}$. This last relation can in fact be obtained analytically [77].
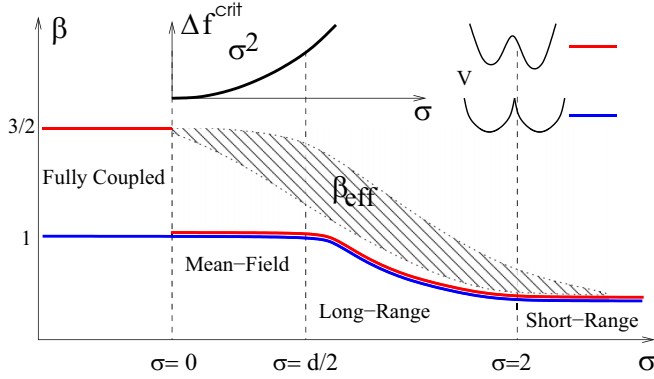
FIG. 10. Red and blue lines show the expected value of β for the two kinds of potentials analyzed. The puzzle posed by the jump of β at $\sigma = 0$ in the continuous case (red line) is solved by noticing that the extent of the critical region for smooth potentials (measured by Δf^{crit}) reduces continuously to zero as $\sigma = 0$ is approached. In the region $\sigma \leqslant 0$ the nonuniversal critical exponent $\beta = 3/2$ is observed. This raises the possibility (in experiments or numerical simulations) to observe strong corrections to scaling in the smooth potential case, especially at low values of σ, that may induce us to adjust effective values of the β exponent (roughly indicated by the hatched region) that are expected to be larger than the true values.

V. CONCLUSIONS

In Fig. 10 we summarize the picture that emerges from our results. The peculiar breakdown of universality in the $\sigma \to 0$ limit is explained in terms of a vanishing critical region for smooth potentials (whenever disorder is strong enough to have a finite f_c in such limits). We argue that the vanishing of the critical region has practical implications for the analysis of long-range depinning. Since the fully coupled model has a $\beta = 3/2$ exponent for smooth potentials, larger than the universal $\beta = 1$ for cuspy potentials, effective values $3/2 > \beta_{\mathrm{eff}} > 1$ are plausible to be observed for $\sigma \gtrsim 0$, but also for even larger σ we expect an excess, i.e., $\beta_{\mathrm{eff}}(\sigma) > \beta(\sigma)$. The difference between the effective and the right exponents are found to be more important for the dynamical exponents, β and z, than for the geometric exponents, ζ and ν. From a simple microscopic model we have shown that this is related to the competition between the characteristic time τ_1 associated to single particle instabilities with the time associated to collective instabilities, $\tau \sim (f - f_c)^{-z\nu}$, which is roughly controlled by the number of active particles involved in the spreading of correlations at lengths $l \sim (f - f_c)^{-\nu}$. This competition is made more clear when we analyze avalanche dynamics in the quasistatic limit.

To illustrate the kind of effects we can expect from the nonuniversal corrections to scaling arising from smooth microscopic pinning potentials, in Fig. 11 we show estimations of β and f_c from the raw data points of Fig. 5 for $\sigma = 1$ corresponding to the variable jump rate case discussed in Sec. III B. We use two fitting methods which are often used in the literature. The best pairs f_c and β are obtained from least squares fits to $\log v = \beta \log(f - f_c) + \mathrm{cte}$, varying the number N_p of points considered, starting from the three lowest values of f. For each case we slowly decrease f_c from the lowest value of f. In Fig. 11(a) we show that for
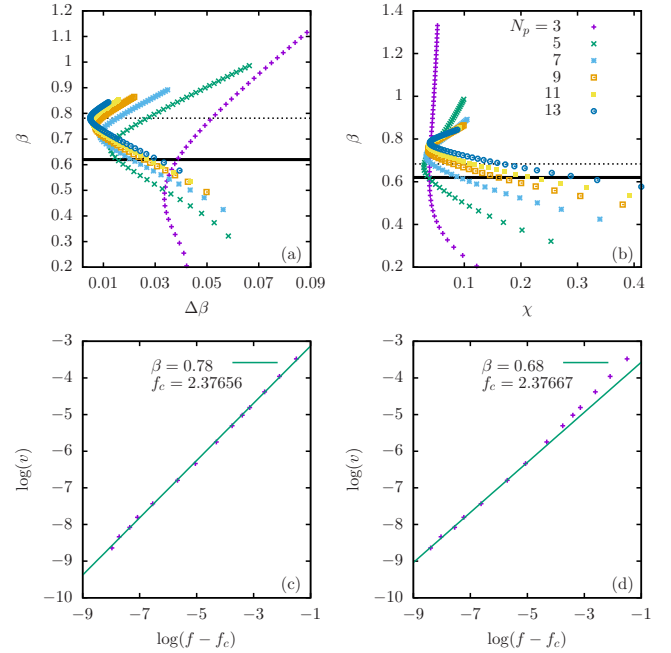

FIG. 11. Estimations of β and f_c from the raw data points of Fig. 5 for $\sigma = 1$ corresponding to the smooth microscopic pinning or variable jump rate case. The best pairs f_c and β are obtained from least squares fits to $\log v = \beta \log(f - f_c) + \mathrm{cte}$, varying the number N_p of points considered from the lowest f. From (a) we choose the values that minimize the fit parameter error $\Delta \beta$ and obtain the fit shown in (c) [the effective β is shown by a dashed line in (a)]. From (b) we choose the values that minimize the standard deviation χ of the fit and obtain the fit shown in (d). (The effective β is shown by a dashed line in (b).] The obtained values must be compared with the asymptotic ones $\beta = 0.62$ [shown with a solid line in (a) and (b)], and $f_c = 2.376\,70$.

each N_p [labels for each N_p are shared with Fig. 11(b)] the fit parameter error $\Delta \beta$ displays a minimum for a given value of f_c. If we choose the values corresponding to this minimum we obtain the fairly good fit of the data shown in Fig. 11(c). If instead we choose the values corresponding to the minimum of the standard deviation χ of the fit we obtain the fit shown in Fig. 11(c). (Note that in this case, the optimum N_p and f_c are different than with the previous criteria.) The obtained values must be compared with those obtained from the more robust constant rate simulations (Fig. 4) $\beta = 0.62$ and $f_c = 2.376\,70$. It is worth noting that in either case the effective β is larger than its true asymptotic value, which is accurately obtained by using the constant rate discrete model.

Our results motivate a reexamination of the empirical experimental and numerical (smooth potential) long-range depinning data analysis. In Ref. [7] the depinning exponent $\beta \approx 0.8$ was directly measured for cracks propagating in an elastic inhomogeneous material. A less direct estimate, also for propagating cracks, can be obtained from the experimental results for the avalanche duration exponent $\gamma = 1.67$ reported in Ref. [46]. Using that $\gamma \approx \beta + \zeta/(1 + \zeta)$ and assuming $\zeta = 0.39$ [44,45], we get $\beta \approx 0.72$. Both values appear to be larger than those predicted for the universality class of one-dimensional elastic interfaces with $\sigma = 1$ long-range elastic

couplings and uncorrelated isotropic disorder, where $\beta \approx 0.63$ [45,46] and $\beta \approx 0.68$ [42] were found numerically using "cuspy" or cellular automata lattice models. One can thus argue that the excess in the effective value of β may arise, in part, from the strong corrections to scaling we expect for long-range depinning with smooth microscopic pinning potentials, due to the vanishing of the critical region approaching the fully coupled limit.

APPENDIX: RESULTS IN HIGHER DIMENSIONS

In addition to considering a long-range interaction in a one-dimensional (1D) system, there is a second standard way to move towards the mean field limit. This is to consider the short-range depinning problem in progressively larger number of dimensions. For short-range interactions, the critical dimension of the depinning problem is $d_c = 4$, i.e., for $d > d_c$ we expect mean field critical exponents, in particular, $\beta = 1$. The short-range case in $d_c = 4$ corresponds to the $\sigma = 1/2$ case of a 1D system. It is then natural to ask if by increasing the dimension d we observe the same trends we observe by decreasing the exponent σ, particularly in the flow curves.

We have found that the answer to this question is affirmative. The relevant results are contained in Figs. 12, 13, and 14 (which should be directly compared to Figs. 4, 5,

FIG. 13. Same as previous figure for variable transition rates.

and 6). There we present simulations of the discrete pinning potential model, in different numbers of spatial dimensions, namely, $d = 1$, 2, 3, 4, and 6, with interactions only among nearest neighbor sites (corresponding to $\sigma \to \infty$). In order to compare different dimensions more easily and to have a well-defined limit as $d \to \infty$, here the elastic interaction G_{ij} [in Eq. (1)] is normalized differently, namely, we take the value of G_{ij} for neighbor sites as $2/d$. The trend we observe as dimension is increased is equivalent to what we have obtained as σ is reduced, in one dimension: For constant rate a robust critical region is obtained and the value of β increases with the number of dimensions, reaching the mean field value $\beta = 1$ for $d = 4$. For variable rates the extent of the critical region is smaller and is reduced as d increases. Note, however,
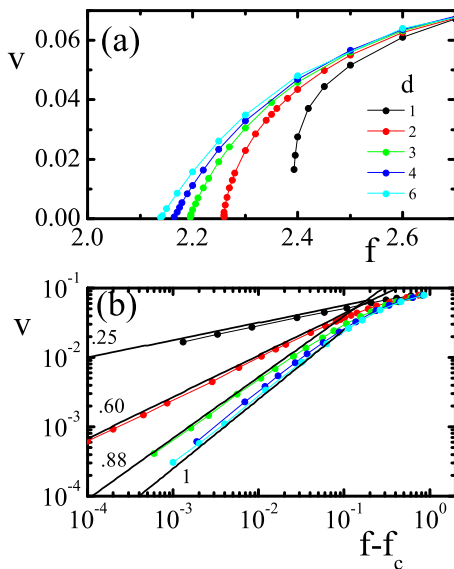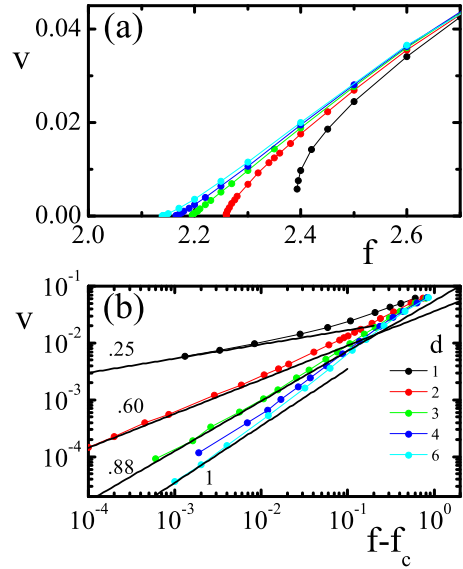

FIG. 12. Velocity as a function of force for interfaces with short-range elasticity and constant transition rate potentials for interfaces of different dimensionality d in linear (a) and logarithmic (b) scale. The fitted values of β are indicated.
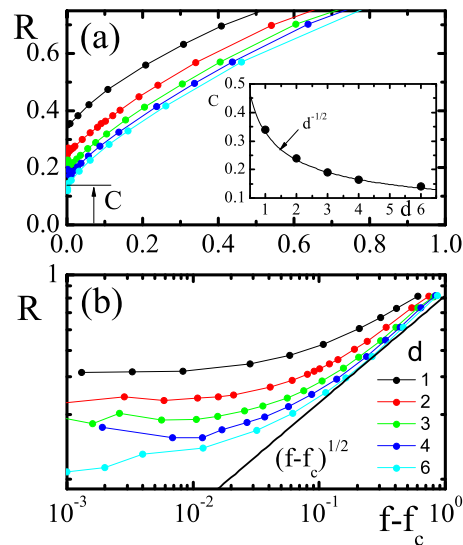

FIG. 14. Ratio between the velocity for variable and constant transition rates. We observe the same trend as obtained in 1D long-range interacting systems as a function of σ (Fig. 6). The value of C decreases with d as $d^{-1/2}$.

that the critical region does not vanish at the upper critical dimension $d = 4$; our data are consistent with the critical region vanishing only as $d \to \infty$ where the mean field value

($\beta = 3/2$) is fully observed. As in the case of varying σ, here we can estimate the extent of the critical region as a function of d (see Fig. 14) and the result is $\Delta f^{\text{crit}} \sim d^{-1}$.

[1] G. Durin and S. Zapperi, in *The Science of Hysteresis: Physical Modeling, Micromagnetics and Magnetization Dynamics*, edited by I. D. Mayergoyz (Cambridge University Press, Cambridge, UK, 2006), Vol. II, Chap. 10.

[2] J. Ferré, P. J. Metaxas, A. Mougin, J.-P. Jamet, J. Gorchon, and V. Jeudy, C. R. Phys. **14**, 651 (2013).

[3] G. Durin, F. Bohn, M. A. Corrêa, R. L. Sommer, P. Le Doussal, and K. J. Wiese, Phys. Rev. Lett. **117**, 087201 (2016).

[4] W. Kleemann, Annu. Rev. Mater. Res. **37**, 415 (2007).

[5] P. Paruch and J. Guyonnet, C. R. Phys. **14**, 667 (2013).

[6] D. Bonamy, S. Santucci, and L. Ponson, Phys. Rev. Lett. **101**, 045501 (2008).

[7] L. Ponson, Phys. Rev. Lett. **103**, 055501 (2009).

[8] J. F. Joanny and P. G. de Gennes, J. Chem. Phys. **81**, 552 (1984).

[9] S. Moulinet, A. Rosso, W. Krauth, and E. Rolley, Phys. Rev. E **69**, 035103 (2004).

[10] P. L. Doussal, K. J. Wiese, S. Moulinet, and E. Rolley, Europhys. Lett. **87**, 56001 (2009).

[11] R. Planet, S. Santucci, and J. Ortín, Phys. Rev. Lett. **102**, 094502 (2009).

[12] S. Atis, A. K. Dubey, D. Salin, L. Talon, P. Le Doussal, and K. J. Wiese, Phys. Rev. Lett. **114**, 234502 (2015).

[13] E. Bayart, I. Svetlizky, and J. Fineberg, Nat. Phys. **12**, 166 (2015).

[14] A. Nicolas, E. E. Ferrero, K. Martens, and J.-L. Barrat, Rev. Mod. Phys. (to be published) [arXiv:1708.09194].

[15] J. P. Sethna, M. K. Bierbaum, K. A. Dahmen, C. P. Goodrich, J. R. Greer, L. X. Hayden, J. P. Kent-Dobias, E. D. Lee, D. B. Liarte, X. Ni, K. N. Quinn, A. Raju, D. Z. Rocklin, A. Shekhawat, and S. Zapperi, Annu. Rev. Mater. Res. **47**, 217 (2017).

[16] T. Nattermann and S. Scheidl, Adv. Phys. **49**, 607 (2000).

[17] T. Giamarchi and S. Bhattacharya, in *High Magnetic Fields*, edited by C. Berthier, L. P. Lévy, and G. Martinez, Lecture Notes in Physics Vol. 595 (Springer Verlag, Berlin, 2002), pp. 314–360.

[18] P. Le Doussal, Int. J. Mod. Phys. B **24**, 3855 (2010).

[19] T. Schulz, R. Ritz, A. Bauer, M. Halder, M. Wagner, C. Franz, C. Pfleiderer, K. Everschor, M. Garst, and A. Rosch, Nat. Phys. **8**, 301 (2012).

[20] O. Chepizhko, C. Giampietro, E. Mastrapasqua, M. Nourazar, M. Ascagni, M. Sugni, U. Fascio, L. Leggio, C. Malinverno, G. Scita, S. Santucci, M. J. Alava, S. Zapperi, and C. A. M. La Porta, Proc. Natl. Acad. Sci. U.S.A. **113**, 11408 (2016).

[21] E. A. Jagla and A. B. Kolton, J. Geophys. Res.: Solid Earth **115**, B05312 (2010).

[22] E. A. Jagla, F. P. Landes, and A. Rosso, Phys. Rev. Lett. **112**, 174301 (2014).

[23] D. S. Fisher, Phys. Rep. **301**, 113 (1998).

[24] M. Kardar, Phys. Rep. **301**, 85 (1998).

[25] L. A. N. Amaral, A. L. Barabsi, and H. E. Stanley, Phys. Rev. Lett. **73**, 62 (1994).

[26] A. B. Kolton, A. Rosso, T. Giamarchi, and W. Krauth, Phys. Rev. Lett. **97**, 057001 (2006).

[27] A. B. Kolton, A. Rosso, T. Giamarchi, and W. Krauth, Phys. Rev. B **79**, 184207 (2009).

[28] V. H. Purrello, J. L. Iguain, A. B. Kolton, and E. A. Jagla, Phys. Rev. E **96**, 022112 (2017).

[29] T. Nattermann, S. Stepanow, L.-H. Tang, and H. Leschhorn, J. Phys. II (France) **2**, 1483 (1992).

[30] O. Narayan and D. S. Fisher, Phys. Rev. Lett. **68**, 3615 (1992).

[31] O. Narayan and D. S. Fisher, Phys. Rev. B **48**, 7030 (1993).

[32] K. Joerg Wiese and P. Le Doussal, Morkov Processes Relat. Fields **13**, 777 (2007).

[33] H. Leschhorn, T. Nattermann, S. Stepanow, and L. Tang, Ann. Phys. **509**, 1 (1997).

[34] E. E. Ferrero, S. Bustingorry, A. B. Kolton, and A. Rosso, C. R. Phys. **14**, 641 (2013).

[35] P. Le Doussal, K. J. Wiese, and P. Chauve, Phys. Rev. B **66**, 174201 (2002).

[36] A. A. Fedorenko and S. Stepanow, Phys. Rev. E **67**, 057104 (2003).

[37] H. Leschhorn, Physica A (Amsterdam) **195**, 324 (1993).

[38] L. Roters, A. Hucht, S. Lübeck, U. Nowak, and K. D. Usadel, Phys. Rev. E **60**, 5202 (1999).

[39] A. Rosso, A. K. Hartmann, and W. Krauth, Phys. Rev. E **67**, 021602 (2003).

[40] A. Rosso, P. Le Doussal, and K. J. Wiese, Phys. Rev. B **75**, 220201 (2007).

[41] E. E. Ferrero, S. Bustingorry, and A. B. Kolton, Phys. Rev. E **87**, 032122 (2013).

[42] S. Ramanathan and D. S. Fisher, Phys. Rev. B **58**, 6026 (1998).

[43] S. Zapperi, P. Cizeau, G. Durin, and H. E. Stanley, Phys. Rev. B **58**, 6353 (1998).

[44] A. Rosso and W. Krauth, Phys. Rev. E **65**, 025101 (2002).

[45] O. Duemmer and W. Krauth, J. Stat. Mech.: Theory Exp. (2007) P01019.

[46] L. Laurson, X. Illa, S. Santucci, K. Tore Tallakstad, K. J. Måløy, and M. J. Alava, Nat. Commun. **4**, 2927 (2013).

[47] H.-H. Boltz and J. Kierfeld, Phys. Rev. E **90**, 012101 (2014).

[48] L.-H. Tang, M. Kardar, and D. Dhar, Phys. Rev. Lett. **74**, 920 (1995).

[49] A. A. Fedorenko, P. Le Doussal, and K. J. Wiese, Phys. Rev. E **74**, 061109 (2006).

[50] S. Bustingorry, A. B. Kolton, and T. Giamarchi, Phys. Rev. B **82**, 094202 (2010).

[51] A. Rosso and W. Krauth, Phys. Rev. Lett. **87**, 187002 (2001).

[52] T. Goodman and S. Teitel, Phys. Rev. E **69**, 062105 (2004).

[53] P. Le Doussal and K. J. Wiese, Phys. Rev. E **67**, 016121 (2003).

[54] Y. J. Chen, S. Zapperi, and J. P. Sethna, Phys. Rev. E **92**, 022146 (2015).

[55] L. E. Aragón, A. B. Kolton, P. L. Doussal, K. J. Wiese, and E. A. Jagla, Europhys. Lett. **113**, 10002 (2016).

[56] A. Glatz, T. Nattermann, and V. Pokrovsky, Phys. Rev. Lett. **90**, 047201 (2003).

[57] We already discard the possible existence of finite-size [78] and other type of crossovers (see, e.g., Refs. [50,54,79]), or thermal rounding effects [28,80,81], which may also make difficult the experimental observation of a clear power law in the velocity-force characteristics.

[58] C. J. Bolech and A. Rosso, Phys. Rev. Lett. **93**, 125701 (2004).

[59] A. B. Kolton, S. Bustingorry, E. E. Ferrero, and A. Rosso, J. Stat. Mech.: Theory Exp. (2013) P12004.

[60] It is interesting in this respect to quote the following statements by Fisher in Ref. [23]: "The velocity exponent, β, in mean-field theory is not fully universal. It depends on whether or not the pinning forces are continuously differentiable and, if not, on the nature of the singularities in $f_p(u)$. For all but discontinuous forces, this causes long timescales in mean-field theory associated with the acceleration away from configurations that have just become unstable. With short-range interactions, these should not play a role due to the jerky nature of $\phi(\mathbf{r}, t)$ caused by jumps. Thus the mean-field models with $\beta_{MF} = 1$ are the *right* ones about which to attempt an RG analysis."

[61] We assume that f_c is not controlled by extreme statistics in the large-size limit [59].

[62] A. A. Middleton, Phys. Rev. Lett. **68**, 670 (1992).

[63] A. Rosso and W. Krauth, Phys. Rev. B **65**, 012202 (2001).

[64] A. Rosso and W. Krauth, Comput. Phys. Commun. **169**, 188 (2005).

[65] A. B. Kolton, G. Schehr, and P. Le Doussal, Phys. Rev. Lett. **103**, 160602 (2009).

[66] The discussion of anisotropic depinning universality classes, where STS is broken, will be published elsewhere. Nevertheless, we believe that our general conclusions hold also for this case.

[67] A. B. Kolton, A. Rosso, E. V. Albano, and T. Giamarchi, Phys. Rev. B **74**, 140201 (2006).

[68] S. F. Edwards and D. R. Wilkinson, Proc. R. Soc. London A **381**, 17 (1982).

[69] P. Chauve, T. Giamarchi, and P. Le Doussal, Phys. Rev. B **62**, 6241 (2000).

[70] The $\sigma = d/2$ case has $\beta = 1$ but with weak logarithmic corrections [36].

[71] V. L. Popov and J. A. T. Gray, in *The History of Theoretical, Material and Computational Mechanics – Mathematics Meets Mechanics and Engineering* (Springer, Berlin, 2014), pp. 153–168.

[72] X. Cao, S. Bouzat, A. B. Kolton, and A. Rosso, Phys. Rev. E **97**, 022118 (2018).

[73] The value for $\sigma = 2$ is somewhat lower than the expected $\beta = 1$; however, this is not surprising in view of the logarithmic corrections expected in this case (see [36]).

[74] We can consider more general rate laws, namely, a rate proportional to $(f - f_c)^q$ with q different from 0 and 1/2. They correspond to different forms of the singularities at the transition points of the continuum potentials, and in this case the properties of the model would be smoothly dependent on the q value. However, we think this kind of singularity in the continuum potentials for other values of q are very artificial, and this is the reason why we use the limits $q = 0$ (cuspy potentials) and $q = 1/2$ (smooth potentials).

[75] In the case of transition rates corresponding to the smooth potential case [i.e., $\sim (f_i^{\mathrm{app}} - f_i^{\mathrm{th}})^{-1/2}$], the activation time diverges for the first site, since $f_i^{\mathrm{app}} = f_i^{\mathrm{th}}$. This diverging triggering time is not considered in the evaluation of T.

[76] I. Fernández Aguirre and E. A. Jagla, Phys. Rev. E **98**, 013002 (2018).

[77] I. Fernández Aguirre, A. Rosso, and E. A. Jagla (unpublished).

[78] O. Duemmer and W. Krauth, Phys. Rev. E **71**, 061601 (2005).

[79] S. Bustingorry and A. Kolton, Pap. Phys. **2**, 020008 (2010).

[80] L.-W. Chen and M. C. Marchetti, Phys. Rev. B **51**, 6296 (1995).

[81] S. Bustingorry, A. B. Kolton, and T. Giamarchi, Phys. Rev. E **85**, 021144 (2012).